PERGAMON

Solid State Communications 113 (2000) 657–662

solid state communications

www.elsevier.com/locate/ssc

Charge density wave formation accompanying ferromagnetic ordering in quasi-one-dimensional $BaIrO_3$

G. Cao[a,*], J.E. Crow[a], R.P. Guertin[b], P.F. Henning[c], C.C. Homes[c], M. Strongin[c], D.N. Basov[d], E. Lochner[e]

[a]*National High Magnetic Field Laboratory, Tallahassee, FL 32310, USA*
[b]*Department of Physics and Astronomy, Tufts University, Medford, MA 02155, USA*
[c]*Physics Department, Brookhaven National Laboratory, Upton, NY 11973, USA*
[d]*Physics Department, University of California, San Diego, La Jolla, CA 92093, USA*
[e]*Center for Materials Research and Technology, Florida State University, Tallahassee, FL 32306, USA*

Received 20 July 1999; accepted 3 November 1999 by E.E. Mendez

Abstract

The magnetic, transport, optical, and structural properties of quasi-one-dimensional $BaIrO_3$ show evidence for the simultaneous onset of electronic density wave formation and ferromagnetism at $T_{c3} = 175$ K. Two additional features in the chain direction dc conductivity show a sudden change to metallic behavior below $T_{c2} = 80$ K and then a Mott-like transition at $T_{c1} = 26$ K. Highly non-linear dc conductivity, optical gap formation at $\approx 9k_BT_{c3}$, additional phonon modes, and emergent X-ray satellite structure support density wave formation. Even at very high (30 T) fields the saturation Ir moment is very small, $\approx 0.04\mu_B$/Ir. © 2000 Elsevier Science Ltd. All rights reserved.

Keywords: A. Magnetically ordered materials; C. Crystal structure and symmetry; D. Electronic transport; D. Exchange and superexchange; D. Optical properties

Transition metal oxides (TMO) with low crystalline symmetry are known to exhibit electronic density wave formation [1–3]. However, to our knowledge, density wave formation has not yet been observed accompanying the onset of ferromagnetic order. However, the ferromagnetism at $T_{c3} = 175$ K in $BaIrO_3$ [4] appears to be accompanied by and possibly driven by a collective electronic excitation or at least partial gapping of the Fermi surface. This demonstrates once again the strong coupling between spin and charge in the heavy (4d- and 5d-based) TMOs [5–7]. $BaIrO_3$ has a highly anisotropic quasi-one-dimensional structure [8–10] and this gives rise, in our single crystal samples, to large anisotropy of $\rho(T)$, the electrical resistivity, with the quasi-one-dimensional axis, the *c*-axis, having much lower resistivity. This kind of low-dimensional structure is necessary for the formation of an insulating charge density wave (CDW) ground state, which is a collective electron mode normally incommensurate with the underlying lattice for partially filled bands [3].

Evidence for density wave formation comes from: (1) A discontinuous increase in the slope of $\rho(T)$ vs. T at $T_{c3} = T_C$, the Curie temperature—an abrupt transition to a more insulating phase. (Two additional features of $\rho(T)$ along the *c*-axis, at $T_{c2} = 80$ K and $T_{c1} = 26$ K, mark a sudden return to "metallic" behavior (possibly a crossover from partial toward full gapping of the Fermi surface) and a well-defined Mott-like metal–insulator transition, respectively). (2) An abrupt feature in the non-linear conductivity showing negative differential resistivity. (3) Gap formation at about 1200 cm^{-1} in the electron excitation spectrum and a splitting of a phonon mode at 350 cm^{-1}, which appear for $T < T_{c3}$ (This was determined by optical reflectivity studies in the far and near infrared.). (4) Additional satellite formation for $T < T_{C3}$ in the X-ray diffraction spectrum.

The structure of $BaIrO_3$ is monoclinic and consists of Ir_3O_{12} trimers of face-sharing IrO_6 octahedra which are vertex-linked to other trimeric clusters forming columns roughly parallel to the *c*-axis. These clusters form channels accommodating Ba ions. The space group is C2/m and the

* Corresponding author.

0038-1098/00/$ - see front matter © 2000 Elsevier Science Ltd. All rights reserved.
PII: S0038-1098(99)00532-3

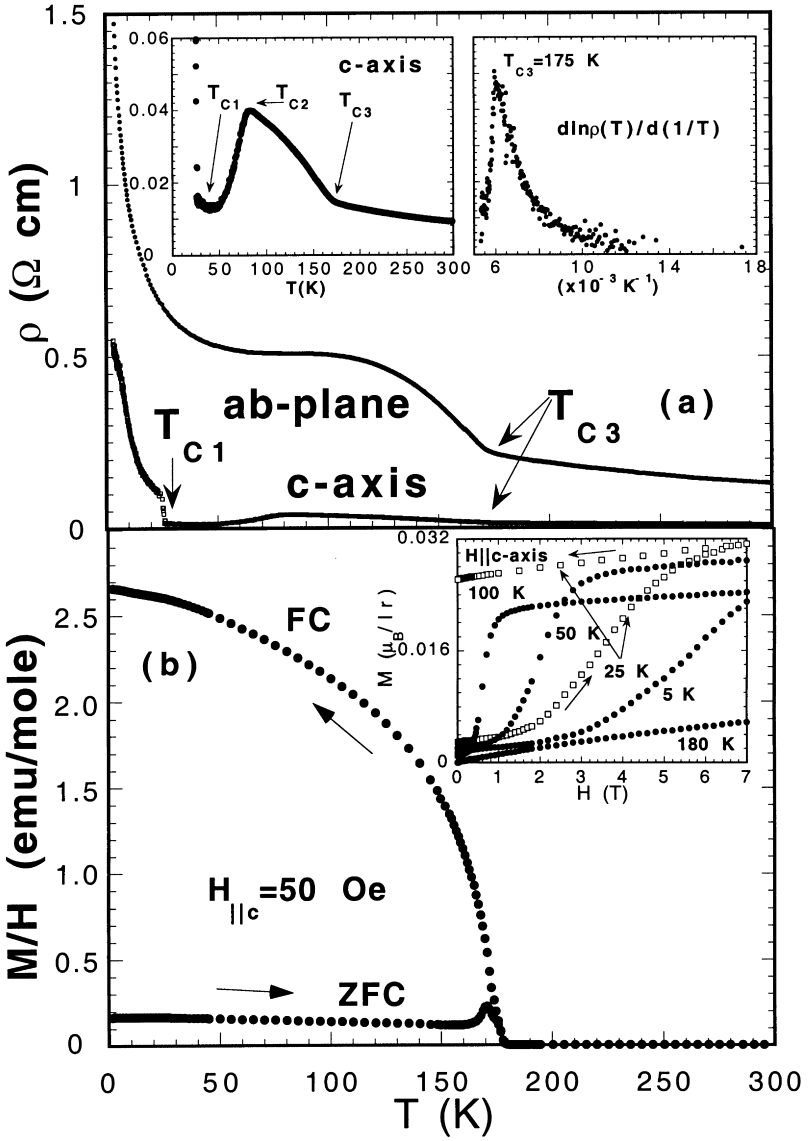

Fig. 1. (a) Electrical resistivity vs temperature for $BaIrO_3$ for the two major crystallographic directions. The first inset shows details of *c*-axis conductivity and the second the sharp peak in d[ln $\rho_{ab}(T)$/d(1/T)] at T_{c3}, which also denotes the onset of ferromagnetism. (b) Field cooled and zero field cooled magnetization showing the onset at $T_{c3} = 175$ K, commensurate with the $\rho(T)$ anomaly. The inset shows isothermal magnetization at several temperatures. Note the large hysteresis, for example, at $T = 25$ K (empty squares).

unit cell parameters are $a = 10.005$ Å, $b = 5.751$ Å, $c = 15.174$ Å and $\beta = 103.274°$ determined from high resolution X-ray diffraction studies [8–10]. Two crystallographically distinct clusters give rise to two different Ir–Ir distances, 2.626 and 2.633 Å, which are shorter than the intercluster distances 3.958 and 3.975 Å and even shorter than the Ir–Ir distances in Ir metal. This allows two types of interactions—direct Ir–Ir bonding for face-sharing and indirect Ir–O–Ir linkages for corner-sharing ocatahedra. The orientation and face sharing of the IrO_6 octahedra plus distortions of the octahedra themselves give rise to a very low symmetry quasi-one-dimensional structure with the *c*-axis being the high conductivity axis. Though direct bonding should broaden the d-bandwidth and result in metallic behavior [11], twisting and buckling of the cluster trimers evidently reduce the bandwidth, because the system is essentially non-metallic, i.e. $d\rho(T)/dT < 0$ except for $26 < T < 80$ K along the *c*-axis.

The $BaIrO_3$ samples were flux grown at relatively low temperatures (1000 K) using $BaCl_2$ as a flux agent. The samples were examined with X-ray diffraction for possible additional phases and none were found within the accuracy

of the measurements, i.e. ≈1%. The stoichiometric ratio of Ba:Ir was determined from energy dispersive X-ray analysis. Magnetic measurements were performed on a Quantum Design MPMS system to 7 T, a vibrating sample magnetometer to 30 T dc fields at the NHMFL, and in a pulsed field magnetometer at the NHMFL—Los Alamos Laboratory Pulsed Field Facility. Resistivity and magnetoresistivity to 10 T were performed with a standard four probe technique. The optical conductivity was obtained from a Kramers–Kronig analysis of polarized reflectance measurements performed with a Brucker 66 spectrometer. Polarized reflectance was measured from 40 to 6000 cm^{-1} and was merged with unpolarized measurements to 19,000 cm^{-1}, above which a $1/\omega^4$ dependence of the reflectance was assumed. All the results shown here were obtained from data on several samples; no sample dependence of any of the properties was found.

The essential transport and magnetic properties of $BaIrO_3$ are summarized in Figs. 1a and b. The first inset of Fig. 1a shows an expanded scale for $\rho_c(T)$. The second inset details $d\ln \rho_{ab}(T)/d(1/T)$ vs $1000/T$ showing a lambda type anomaly at the ferromagnetic ordering temperature, T_{c3}. This is strikingly similar to that seen in the CDW forming material $(TaSe_4)_2I$ (Ref. [3]). The anisotropy of $\rho(T)$ is easily seen in Fig. 1a: For example, $\rho_{ab}/\rho_c \approx 40$ for $T = 27$ K. The transition at T_{c3} in $\rho_{ab}(T)$ is abrupt and the steady increase of $\rho_{ab}(T)$ suggests progressive localization of charge carriers. The discontinuity in $\rho_c(T)$ at T_{c1} is a metal–nonmetal transition connecting metallic-like behavior for $T_{c1} < T < T_{c2} \approx 80$ K with non-metallic for $T < T_{c1}$ ($\rho_c(2\text{ K})/\rho_c(27\text{ K}) \approx 55$). This transition is nearly identical to that seen in the bilayered 4d TMO $Ca_3Ru_2O_7$ [5,6], though the comparable discontinuity in $\rho(T)$ for $Ca_3Ru_2O_7$ at $T_M = 48$ K is not restricted to one principal axis as in $BaIrO_3$. It is noted that $\rho_C(T)$ in the metallic state ($30 < T < 80$ K) is larger than the Mott limit. Such "bad metal" behavior is commonly seen in many other transition metal oxides such as cuprates, manganites, ruthenates.

Extracting a gap in the excitation spectrum from the data of Fig. 1a is problematic because activated resistivity would be expected for $T \ll T_{CDW}$ and in this temperature range for $BaIrO_3$ we see additional features in $\rho_c(T)$ which could easily mask the activated behavior. Attempts to fit $d\rho(T)/dT$ for $T \leq T_{C3}$ to $d\rho(T)/dT \propto (1/T_{C3}^2)(T_{C3} - T)^{-1/2}$ were only moderately successful, possibly for the same reason [3]. We suggest the transition from insulating to metallic conductivity at T_{c2} may represent a crossover from partial gapping of the Fermi surface at T_{c3} toward eventual full gapping at T_{c1}.

Although $\rho(T)$ is not strictly "metallic" or even temperature independent above $T_{c3} = 175$ K as might be expected for temperatures above a density wave transition, such a high temperature "near metallic" phase is also found in TaS_3 and $(TaSe_4)_2I$ and is attributed to fluctuation effects which become very important in low dimensional systems (Ref. [3, Fig. 3.10]).

Most significant for the purpose of this paper is that the transition at T_{c3} is accompanied by the onset of ferromagnetism (Fig. 1b). This transition temperature is unchanged and the resistivity anomaly (Fig. 1a) is not broadened in fields even up to 10 T, unlike most ferromagnetic transitions which are accompanied by short range magnetic order for $T \geq T_C$. This implies that the ordered magnetism is driven by CDW formation or partial Fermi surface gapping accompanied by a subtle lattice distortion at T_{C3}, as indicated by anomalies in the temperature dependence of X-ray diffraction spectrum[1] and a splitting of a phonon mode below 180 K (see inset in Fig. 3b).

The ordered Ir moment $\mu_0 \approx 0.03\mu_B$/Ir. Such a small Ir moment in $BaIrO_3$ is probably intrinsic due to d–p hybridization and small exchange splitting, rather than spin canting from a localized full-moment antiferromagnetic spin configuration [4]. This is based not only on the low value of the effective moment, but also on our magnetization measurements to 30 T dc fields at several temperatures $5 \leq T \leq 200$ K. No higher field induced transitions were found and full saturation to $\mu_0 \approx 0.03\mu_B$/Ir was not achieved until 20 T for $T = 5$ K. Higher pulsed field magnetization measurements to 55 T also do not show any field induced transitions. From a modified Curie–Weiss fit to the data for $T_{c3} < T < 400$ K, the effective paramagnetic moment of the Ir ion is $\mu_{eff} \approx 0.13\mu_B$/Ir and the Curie–Weiss temperature, $\Theta \approx 175$ K, matched T_{C3}. The Ir moment is much lower than expected for the low spin $S = 1/2$, $^2T_{2g}$ state of Ir^{4+} ($5d^5$) which has degenerate d_{xz} and d_{yz} orbitals and an excited half filled d_{xy} orbital, but both T_C and the moment value are in substantial agreement with the results of Lindsay et al. [4] for polycrystalline material. Similar low Ir moments are found for ferromagnetic Sr_2IrO_4 ($T_C = 250$ K, $\mu_{eff} = 0.04\mu_B$/Ir) as well as for $CaIrO_3$ and Ca_2IrO_4 [7,12].

The modified Curie–Weiss law analysis of $\chi(T)$ yielded a rather large temperature independent susceptibility, $\chi_0 = 1.5 \times 10^{-4}$ emu/mol, comparable to that of highly enhanced metal systems such as Pd, which is surprising because it denotes a large density of states at the Fermi surface, $N(E_F)$, at least for $T > T_{C3}$. A more direct measurement of $N(E_F)$ from our own measurements of the low temperature specific heat ($1 \leq T \leq 20$ K) gave a very small value for the electronic specific heat coefficient, $\gamma \approx 1$ mJ/mol K^2. The enhancement of χ_0 without a parallel increase in γ indicates a Stoner enhancement, consistent with the observed ferromagnetic ground state and/or a change in the Fermi surface brought about by the ferromagnetic/CDW transition at T_{C3}. The decrease in $N(E_F)$ is also indirect evidence for gap

[1] Additional X-ray diffraction lines emerge for $T < T_{c3}$ for the following indices: (−111), (111), (113), (224) (131) and (620). (−111) and (111) merge as a broad peak, (113) grows without a shift in 2Θ, and (131) splits into two peaks. As expected for CDW formation, all these changes are subtle and yet well defined, however, indicating no major crystal symmetry alterations.

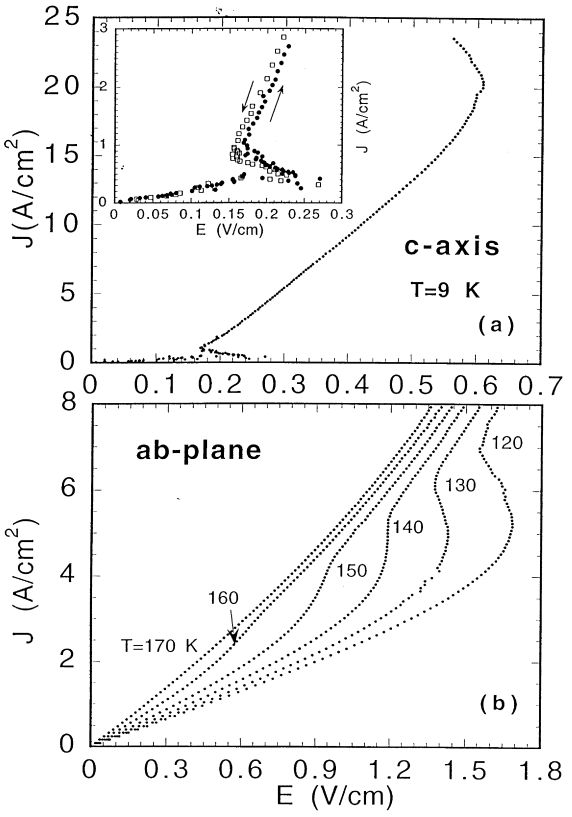

Fig. 2. Non-linear current–voltage characteristics for current along (a) the *c*-axis and (b) the *ab*-plane. The inset shows details of the noisy I–V characteristics at low current and the ohmic behavior for $I < 2$ mA.

formation at the Fermi surface for $T < T_{C3}$ and is supported by optical studies discussed below.

Some zero field cooled isothermal magnetization data are shown in the inset of Fig. 1b for H ∥ *c*-axis. The magnetic anisotropy driven critical fields explain the zero field cooled data in Fig. 1b, a robust feature which was also seen by Powell and Battle [8]. The critical transition fields for H ⊥ *c*-axis are larger, supporting the *c*-axis as close to the easy axis for ferromagnetic alignment. In addition, magnetic saturation for H ⊥ *c*-axis was about 15% smaller than for H ∥ *c*-axis. The $M(H)$ is extremely hysteretic: When the field is reduced to $H = 0$ T, the magnetization remains essentially unchanged from the saturation value (see inset in Fig. 1b). Surprisingly, we see that there is no apparent anomaly in the low field magnetization at the metal–insulator transition at $T_{c1} = 26$ K [13] even for H ∥ *c*-axis.

Non-linear conductivity is a prominent feature of CDW systems. They represent a collective charge transport mode with the CDWs depinned and sliding relative to the underlying lattice, depinned not only by thermal energy but by an external electric field. We show representative current–voltage characteristics of $BaIrO_3$ for current both parallel (Fig. 2a) and perpendicular (Fig. 2b) to the *c*-axis. The striking non-ohmic "S" shape illustrates current controlled negative differential resistivity [14] (NDR) over a wide range of currents and temperatures, but restricted to $T < T_{C3}$. We stress this as a bulk effect, similar in that respect to the Gunn effect, which, however, displays "N" shaped, voltage controlled NDR I–V characteristics [15]. "S" NDR has been found in three other systems: $Ca_3Ru_2O_7$ [16], Sr_2IrO_4 [7], and Ca_2IrO_4 [7] also below their respective magnetic ordering temperatures. The non-hysteretic large main feature of

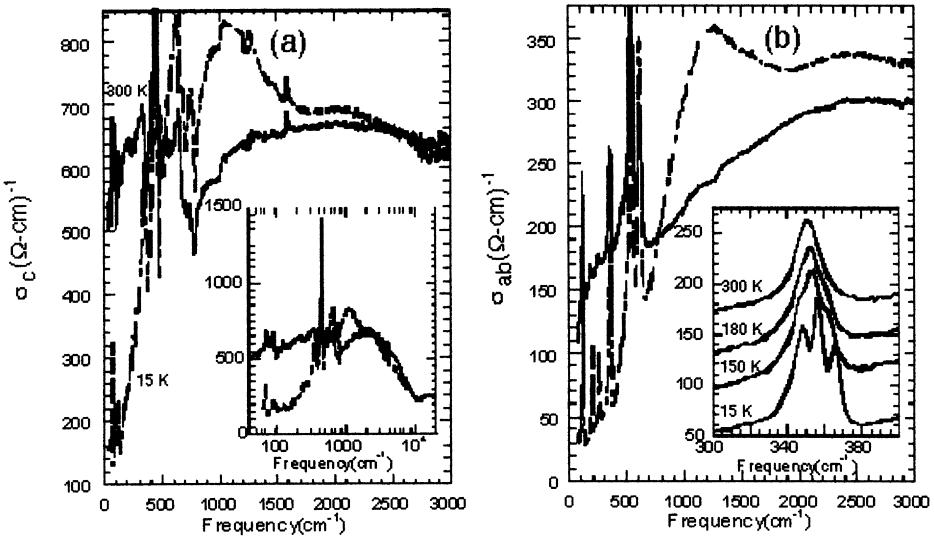

Fig. 3. Optical conductivity (a) parallel and (b) perpendicular to the *c*-axis at 300 K (smooth line) and 15 K (dashed line). For $T < T_{c3}$, an additional broad peak emerges in the vicinity of 1200 cm^{-1} for both polarizations. The inset (a) shows $\sigma_c(\omega)$ out to 19000 cm^{-1}, illustrating the broad polaronic peak at 2100 cm^{-1}, and inset (b) shows the splitting of a room temperature *a*/*b*-axis phonon mode at 350 cm^{-1} below T_{c3} (300, 180, 150, and 15 K curves are shown).

non-linearity of the I–V characteristics may be due to an electrothermal effect which can occur in systems with $d\rho(T)/dT < 0$ if the heat sinking to ambient temperature is insufficient to remove joule heating. (Recently, Young et al. [12] found $T_C \approx 600$ K and $\approx 0.001\mu_B/x$ in $Ca_{1-x}La_xB_6$ for $x \approx 0.005$. Whether a similar dilute electronic gas mechanism accounts for the iridate anomalies remains an open question.) However, the sharp, hysteretic feature in Fig. 1a cannot be a thermally related effect, and we attribute it to current induced CDW depinning for $T \ll T_{c3}$.

Measurements of the optical conductivity (Fig. 3a and b) have been performed as a direct probe of the CDW gap. The room temperature conductivity is strongly anisotropic with the extrapolated conductivities $\sigma_c(0)/\sigma_{ab}(0) \approx 8$, in good agreement with dc measurements. Conductivity both parallel and perpendicular to the chains shows marked non-Drude behavior, and a broad peak in the conductivity is observed along the *c*-axis in the vicinity of 2100 cm^{-1} (260 meV). This broad peak and the insulating-like behavior of σ_c at low frequencies suggests that a polaronic channel dominates the conduction at these temperatures [17]. A gap defined by the onset at $E_g = 1055\ cm^{-1}$ (131 meV) along the *c*-axis and 1200 cm^{-1} (150 meV) along the *ab*-plane emerges below 180 K. This corresponds to $E_g \approx 9k_BT_c$, larger than the predicted value of $3.54k_BT_c$ for a mean-field Peierls transition but close to the size of the gap measured in other CDW systems [18]. The opening of the gap is accompanied by a sharp peak just above the gap edge, a common and predicted feature of CDW systems [18–22] such as the one-dimensional organic conductor $(TMTSF)_2ReO_4$, which has a CDW transition at 175 K and corresponding gap at 1500 cm^{-1} [23], and where $BaBiO_3$ is an example of another oxide system [19]. In the inset to Fig. 3b we show another consequence of the CDW transition, which is the splitting of a phonon mode along the ab-plane at 350 cm^{-1} into at least three features below 180 K, a signature of the removal of degeneracy associated with this symmetry-breaking transition. This structural feature, coupled with the X-ray data which shows additional superstructure peaks below 180 K, are strong evidence against ascribing the transition at T_{c3} to spin density wave formation.[1]

The linear and non-linear transport, magnetism, and optical conductivity data presented here on $BaIrO_3$ give strong evidence for a distortion-precipitated charge density wave formation with the simultaneous onset of weak ferromagnetism at $T_{c3} = 175$ K. To our knowledge this is the first such transition observed. (Simultaneous magnetic and structural transitions are also seen in some 4f systems, where aspherical Coulomb scattering drives the ordered magnetism [24].) The abrupt features at T_{c1} and T_{c2} then may result from a charge ordered state arising from small polaron formation and/or CDW formation in this low dimensional system—perhaps a "small polaron CDW" [25]. The $T_{c1} = 26$ K anomaly adds $BaIrO_3$ to the small group of materials showing a spontaneous temperature-driven metal–insulator transition. Like the organic charge transfer salts, the density wave formation is highly anisotropic, as the 26 K transition is absent for current perpendicular to the chain axis. The intimate connection between the onset of ordered magnetism and the CDW formation in 4d and 5d TMOs deserves further investigation.

Acknowledgements

The authors are pleased to acknowledge useful discussions with L. Gor'kov, V. Dobrosavljevic and J. Brooks. The work was supported by the National Science Foundation under Cooperative Agreement no. DMR95-27035 and DMR98-75980 and the State of Florida. Support is also acknowledged from USDOE, Division of Materials Science, under contract no. DE-AC02-98CH10886.

References

[1] G. Travaglini, P. Wachter, Solid State Commun. 37 (1981) 599.
[2] D.C. Johnston, K. Maki, G. Gruner, Solid State Commun. 53 (1985) 5.
[3] G. Gruner, Density Waves in Solids, Addison-Wesley, Reading, MA, 1994.
[4] R. Lindsay, W. Strange, B.L. Chamberland, R.O. Moyer Jr., Solid State Commun. 86 (1993) 759.
[5] G. Cao, S. McCall, J.E. Crow, R.P. Guertin, Phys. Rev. Lett. 78 (1997) 93.
[6] G. Cao, V. Dobrosavljevic, S. McCall, J.E. Crow, R.P. Guertin, Physica B. 259–261 (1999) 951.
[7] G. Cao, J. Bolivar, S. McCall, J.E. Crow, R.P. Guertin, Phys. Rev. B 57 (1998) 11039R.
[8] A.V. Powell, P.D. Battle, J. Alloy Compounds 191 (1993) 313.
[9] A. Gulino, R.G. Egdell, P.D. Battle, S.H. Kim, Phys. Rev. B 51 (1995) 6827.
[10] T. Siegrist, B.L. Chamberland, J. Less-Common Metals 170 (1991) 93.
[11] P.A. Cox, Transition Metal Oxides: An Introduction to their Electronic Structure and Properties, Clarendon Press/Oxford University Press, Oxford, UK, 1995.
[12] D.P. Young, D. Hall, M.E. Torelli, Z. Fisk, J.L. Sarrao, J.D. Thompson, H.-R. Ott, S.B. Oseroff, R.G. Goodrich, R. Zysler, Nature 397 (1999) 412.
[13] C. Sekine, T. Uchiumi, I. Shirataniani, T. Yagi, Phys. Rev. Lett. 79 (1997) 3218.
[14] M.P. Shaw, V.V. Mitin, E. Scholl, H.L. Grubin, The Physics of Instabilities in Solid State Electron Devices, Plenum Press, New York, 1991.
[15] J.B. Gunn, Solid State Commun. 1 (1963) 88.
[16] R.P. Guertin, J. Bolivar, G. Cao, S. McCall, J.E. Crow, Solid State Commun. 107 (1998) 264.
[17] D. Emin, Adv. Phys. 24 (1975) 305.
[18] C.S. Jacobson, H.J. Pedersen, K. Mortensen, G. Rindorf, N. Thorup, J.B. Torrance, K. Bechgaard, J. Phys. C 15 (1982) 2651.
[19] S.H. Blanton, R.T. Collins, K.H. Kelleher, L.D. Rotter, Z.

Schlesinger, D.G. Hinks, Y. Zheng, Phys. Rev. B 47 (1993) 996.
[20] A.V. Puchkov, T. Timusk, D.A. Payne, Phys. Rev. B 52 (1995) R9855.
[21] R. Bozio, M. Meneghetti, C. Pecile, Phys. Rev. B 36 (1987) 7795.
[22] A.W. McConnell, B.P. Clayman, C.C. Homes, M. Inoue, M. Negishi, Phys. Rev. B 58 (1998) 13565.
[23] C.C. Homes, J.E. Eldridge, Phys. Rev. B 42 (1990) 9522.
[24] H.-R. Ott, Crystalline Electric Field and Structural Effects in f-Electron Systems, Plenum Press, New York, 1980.
[25] V.N. Kostur, P.B. Allen, Phys. Rev. B 56 (1997) 3105.